Numerical simulation of dual oscillating cylinders under different angles for ocean engineering

Peisen Tan[1]
College of Oceanic and Atmospheric Sciences
Ocean University of China
Qingdao, China
tanpeisen@stu.ouc.edu.cn

Dixia Fan[1*]
Department of Mechanical Engineering
Massachusetts Institute of Technology
Cambridge, USA
dfan@mit.edu

***Abstract*—Numerical simulations based on Boundary Data Immersed Method have been performed to study sinusoidal oscillation of an identical pair of circular cylinders under various angle and gap configurations in the still fluid. Simulations on single cylinder cases have also been performed for comparison. An obvious drag force coefficient's increase has been observed especially under large angles. This phenomenon has later been confirmed by calculating energy outflow through a selected control volume. Moreover, double oscillation frequency has been found for the lift force coefficient at all the angles except 45°, at which it has the same frequency as that of motion. Through flow field visualization, these phenomena are explained by discovering two different flow patterns that take place depending on the angle. The first pattern is the vortex circulation pattern when the angle is smaller than 45° while the second pattern is the jet flow pattern when the angle is bigger than 45°. The circulation of vortex around the upper cylinder after being shed out is observed in the vortex circulation pattern, while the jet flow pattern suggests that jet flow is generated in the gap which will be expelled far away and strengthen the energy outflow and dissipation. However, 45° is a critical condition under which the vortex can neither circulate nor shed far in the gap, making the oscillation frequency of lift force almost equal to that of motion.**

Keywords—dual cylinders; oscillation; numerical simulation; angles; lift force coefficient; drag force coefficient

I. INTRODUCTION

The study of oscillating cylinders in still fluid has been attached with great importance because of its significant hydrodynamic value as well as its prevailing presence in ocean engineering. This simplified model can be seen in pump tower made of 3 major cylinders under sloshing loads in Liquefied Natural Gas ships caused by ship rolling in the waves, the oscillation of slender marine risers for marine oilfield exploitation in deep water and the vibration of Blow-Out-Preventer near the seabed where the fluid velocity is close to 0. Under such conditions, the Vortex-Induced-Vibration (VIV) can cause large stresses and fatigue damage on cylinder-like marine structures, thus it can greatly influence the lifespan and maintenance of ocean engineering facilities. The key problem of this study narrows down to the hydrodynamic forces on the cylinder-like structure as well as the flow pattern around them. According Morison Equation (1950), proposed by Morison, Johnson and Schaaf [1], the in-line force on cylinders in oscillatory flow can be expressed as,

$$F_{in-line} = \frac{1}{2}\rho D C_d |U|U + \frac{1}{4}\pi\rho D^2 C_m \frac{du}{dt} \qquad (1)$$

while the lift force could be expressed as,

$$F_{lift} = \frac{1}{2}\rho U^2 D C_l \qquad (2)$$

In (1) and (2), C_m is the added mass coefficient, C_d is the drag force coefficient and C_l is the lift force coefficient. These three non-dimensional crucial coefficients mainly rely on three non-dimensional parameters, the Keulegan-Carpenter (KC) number, the Strokes number (β) and gap ratio (G/D). The KC number is defined as $KC=U_mT/D$, where U_m, T are the maximum oscillatory velocity and the oscillation period. The KC number could be simplified as $KC=2\pi A/D$ for pure sinusoidal motion. The Strokes number(β) is defined as $\beta=D^2/Tv$, where ν is the kinematic viscosity of the fluid. β can also be expressed as $\beta=Re/KC$, as Reynolds number is expressed as $Re=U_mD/\nu$. The gap ratio is defined as *Gap/Diameter* or *G/D,* which is used to demonstrate the relative distance between the cylinders. Other parameters in Morison Equation are ρ (the density of fluid), U (the velocity of oscillation), D (the diameter of the cylinders used in the experiment) and G (the distance between cylinders' centers).

Numerous studies on cylinders under sinusoidal oscillation had been carried out. Bearman (1985) obtained the total force on a single circular cylinder when KC varies from 4-55 and Reynolds number from 100 to 1665 in his experiments [2]. His study showed a precise prediction on the drag force coefficient when KC is smaller than 2. But in the higher KC range, drag coefficient is found to be directly proportional to the KC number. Later, Sarpkaya (1986) also conducted experiments on single cylinders and confirmed that C_d and C_m match with the theory under the critical KC number at which flow transits into unstable condition and depends on the different β for the smooth cylinders [3]. Williamson (1985) visualized the flow field and revealed the KC's effect on the number of the vortex formation. In his study, single pair to four pairs of vortex shedding is reported depending on the KC value [4].

Meanwhile, numerical simulations have been performed to study the hydrodynamic forces as well as the flow field around

978-1-5386-4814-8/18/$31.00 ©2018 IEEE

oscillating cylinders. An, Cheng and Zhao (2009) simulated a cylinder in oscillatory flow with both 2D and 3D finite element models at *Re* of 2000 and *KC* of 1, 2, 5, 10, 17.5, 20 and 26.2. Their study showed that, compared to the 3D model, the 2D model is able to capture the majority of the genuine flow structures as well [5]. Fan (2017) performed numerical simulation of dual cylinders under side-by-side arrangement to verify and explain the enhancement of drag force coefficient under side-by-side arrangement [6]. Zhang(2017) performed a two-dimensional numerical study of dual cylinders under tandem arrangement in still water at relatively low Reynolds number and discovered a 'magnet' effect and the connection of vortex wake under small gap ratio of tandem arrangement [7].

If we define the angle between oscillation direction and cylinder pair's center line as α, then under the side-by-side configuration, α=90º while under tandem arrangement, α=0º. As cylinder-like infrastructures in ocean engineering are very common and are not only aligned in 90º and 0º , but in other angles such as 30º 45º 75º as well, learning the hydrodynamics of cylinders under different angles can be very essential. However, related researches are much rarer and far more complex. In this study, we performed extended numerical simulation and flow visualization for cylinders under different α, which is set from 0º-90º at an interval of 15º. The other key parameters are *KC* number, which is set to 4, 6, 8 respectively. The Reynolds number is fixed to 120 and the Strokes number (β) is adjusted according to *Re* and *KC* as $\beta=Re/KC$. The gap ratio (*G/D*) is set to 0.5, 1.0, 2.0 and 3.0. The simulation extracts real-time data of hydrodynamic forces as well as cylinder's motion and flow field under each condition. Single cylinder cases under each *KC* number are also simulated for comparison. Through flow field visualization, we discovered two typical flow patterns according to α under *KC* of 4 and managed to explain the influence of α on drag force coefficient and lift force coefficient.

II. Simulation Setup

The coordinate system set in this paper is defined in Fig. 1. The cylinder pair oscillates along the *x*-axis with the displacement expression of $x=Asin(\omega t)$. Then the direction of the in-line force is also along the *x*-axis, while the lift force is along the *y*-axis which is vertical to the in-line force.

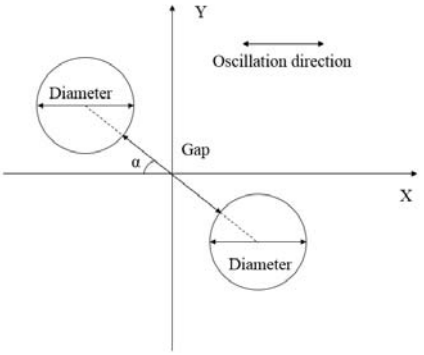

Fig. 1. Simulation setup

The solver used in this paper is called Lily-Pad which is based on Boundary Data Immersed Method (BDIM). Developed by Weymouth and Yue (2011) [8], it was conducted to solve the problems of immersion of solid bodies within a fluid with general boundary conditions. As Fan (2017) has pointed out, this method is based on a general integration kernel formulation which combines the field equations of each domain and the interfacial conditions analytically. The resulting governing equation for the complete domain preserves the behavior of the original system in an efficient Cartesian-grid method, including stable and accurate pressure values on the solid boundary [6].

All the parameters in simulation are non-dimensionalized as $(x,y)=(x',y')/D$, $(u,v)=(u',v')/U_m$, $p=p'/\rho U_m$, and $t=U_m t'/D$. (x,y) are the coordinates in Cartesian mesh. (u,v) are the velocity components in *x* and *y* direction respectively. *t*, *p*, ρ and U_m are time, pressure, density of the fluid and cylinder pair's maximum oscillation velocity in the simulation. The two-dimensional numerical simulation set-up is shown in Fig.1. A control volume is added to the calculation domain to help track and record the energy dissipation on the boundary of the volume. To satisfy the calculation requirement of large motion amplitude and precisely capture the energy outflow from the cylinders, the size of control volume is set to be $4D\times8D$. The boundary effect and blockage effect could affect the computation result, which is quite influential in this study. In order to avoid such disturbance, the size of the calculation domain is set to be $40D\times20D$. The pixel of the screen will directly be nodes of the mesh to establish unstructured meshes, but the size of cylinders and domains with the unit of pixel still have to be defined. In this paper, the diameter (*D*) of every cylinder is set to be 50 pixels, which is appropriate for the calculation domain.

To ensure the reliability and accuracy of the calculation results, a mesh dependency and accuracy study have been conducted with single cylinder cases. The diameter to mesh ratio (δ) we used in verification cases are 40, 50 and 60. In this paper, our results are compared with Zhao Ming's (2005) calculation results [9]. The (*KC, Re*) in Zhao Ming's research is set to be (5,100). For further comparison, we calculate the C_m and C_d under the same *KC* and Reynolds number in three meshes with the diameter to mesh ratio of 40, 50 and 60. The comparison is shown in Table.2. C_m calculated from Mesh4 (δ=40) is 2.29, which is bigger than 2.11, Zhao Ming's result. Meanwhile, C_d from Mesh4 is smaller than Zhao's result. C_m and C_d calculated from Mesh5 where the mesh ratio is 50 are both slightly smaller than Zhao Ming's results. C_d from Mesh6 is bigger than Zhao Ming's results while C_m from Mesh6 is smaller than Zhao Ming's. C_m from Mesh5 is closer to Zhao's results compared with Mesh6 and Mesh4, although C_d from Mesh6 and Mesh5 both have no significant differences from Zhao Ming's result. Thus, Mesh5 matches better with Zhao Ming's results.

Also, in dependency study, the absolute relative deviation (E_{Cm} , E_{Cd} *and* E_{Cl}) from the results calculated by Mesh6 is shown in Table.2. The absolute relative deviation for C_m decreases from 11.7% to 1.5% when δ increases from 40 to 50. The relative deviation for C_d also decreases from 8.5% to 0.8% in the same comparison. Thus, the results show convergence

with the increase of δ and only slight differences are observed between the results from Mesh5 and Mesh6. Fig.2 below shows the fully-developed flow field under Mesh4, Mesh5 and Mesh6. Clear vortex streets on both sides of the cylinder pair could be observed in Mesh5 and Mesh6. However, in Mesh4, the vortex street in flow field further away is not fully captured and demonstrated, which might add difficulties in the observation of flow patterns and the calculation of energy out-flux carried by the vortex.

As meshes with bigger δ also require a longer calculation time, in order to ensure accuracy and efficiency, we choose Mesh5 (δ=50) as the final selection on which our results are calculated in this paper.

TABLE.I. MESH ACCURACY VERIFICATION

	Mesh	δ	C_m	C_d
Zhao Ming[9]	Mesh1	333	2.11	2.43
	Mesh2	1000	2.11	2.43
	Mesh3	1333	2.11	2.42
Current simulation	Mesh4	40	2.29	2.23
	Mesh5	50	2.08	2.42
	Mesh6	60	2.05	2.44

TABLE.II. MESH DEPENDENCY VERIFICATION

	δ	C_m	E_{Cm}	C_d	E_{Cd}
Mesh4	40	2.29	11.7%	2.23	8.5%
Mesh5	50	2.08	1.5%	2.42	0.8%
Mesh6	60	2.05	/	2.44	/

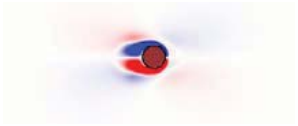

(a)Mesh4(δ=40)

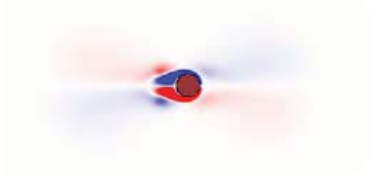

(b)Mesh4(δ=50)

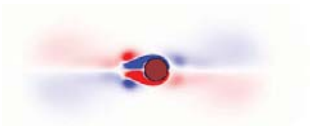

(c)Mesh4(δ=60)

Fig.2. Flow visualization for Mesh4, Mesh5 and Mesh6 (*KC*=5)

III. RESULTS AND DISCUSSIONS

A. Lift Force Coefficient

In this paper, the real-time lift force coefficient during the oscillation is extracted from the simulation. All the results in this paper are calculated based on data of more than 60 periods excluding the initial 20 periods when the vortex flow has not developed fully to guarantee the representativeness of the final calculation results. As the two cylinders are identical and each cylinder is able to represent the hydrodynamics of the flow field, the left-handed cylinder (called Cylinder1) is chosen and mainly analyzed. The right-handed cylinder is referred as Cylinder2 later in the paper. Fig.3 shows the average C_l of Cylinder1 during the oscillation under different α. Both positive and negative phase of C_l are observed (being positive signifies lift force is pointing up while being negative signifies pointing down). Also, when α=0°, C_l can barely be observed, which implies that the lift force is very small under tandem arrangement. The same phenomenon has been discovered by Zhang (2017), who pointed out from the numerical simulation that vortex induced by the left cylinder has a 'magnet' effect on vortex induced by the right cylinder and this 'magnet effect' has a significant restriction on the asymmetry development of the vortex, thus C_l under such cases are relatively small [7].

When α increases, the average C_l reaches a peak at around 30°. Then the lift force decreases and obtains negative value when α=30°-45°, which implies a change of direction for the lift force. This means the average lift force on Cylinder1 when α=15°-45° has opposite direction compared to the average lift force on cylinder1 when α=60°-90°.

The cylinder's real-time oscillatory position and lift force coefficient when *KC*=4 are recorded in Fig.4. The upper graph in fig.3 shows the cylinder position with time while the lower graphs individually show the lift force coefficient with time when α=15°, 45°, 75° and 90°. From Fig.4, higher oscillation frequency has been observed for C_l under all selected α except 45°, where C_l's frequency is lower and almost equals to that of cylinders' motion.

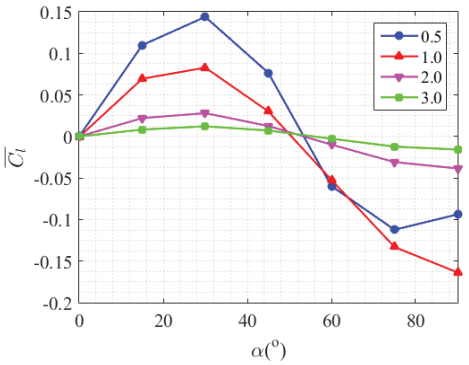

Fig.3. Average Lift force coefficient (*KC*=4)

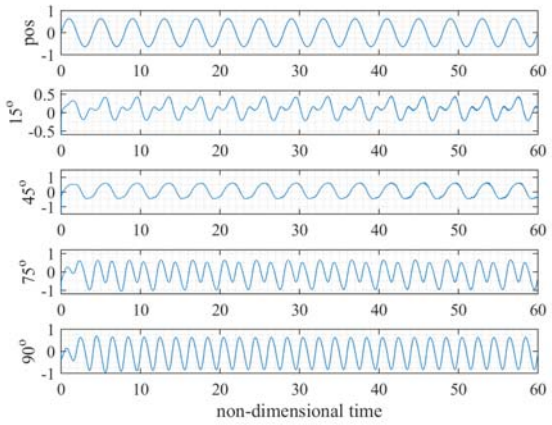

Fig.4. Real-time lift force coefficient vs cylinder position

In this paper, Fast Fourier Transform (FFT) based on real-time data of lift force coefficient is conducted for each α to help analyze the frequency constituents in the oscillation of lift force. Fig.5, Fig.6, Fig.7 and Fig.8 individually shows the Fourier spectrum of C_l and cylinder's motion when α=15°, 45°, 75° and 90° under *KC* of 4. The *x*-axis implies the non-dimensional frequency of C_l. Two obvious frequency peaks are observed for all α except 45° and 90°. The first peak is around the non-dimensional frequency of 0.23-0.25 under which the cylinder pair oscillates. Later in the paper, this frequency is defined as 1st frequency. The second peak is around 0.47-0.51. Later in the paper, it is defined as 2nd frequency. However, C_l's spectrum of 45° only shows a dominating 1st frequency. The 2nd and 3rd frequency are relatively small, which means the oscillation of lift force mainly consists of 1st frequency under the 45° arrangement. On the opposite, when α=90°, the oscillation of lift force has a dominating 2nd frequency, while the 1st frequency can barely be observed.

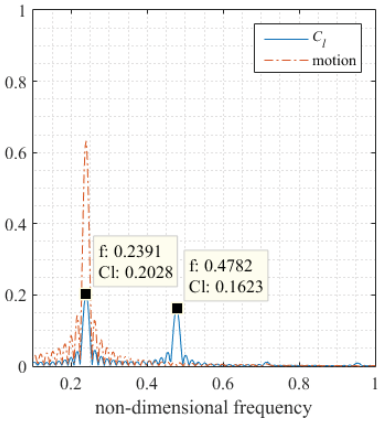

Fig.5. FFT analysis results (*KC*=4, α=15°, *G/D*=0.5)

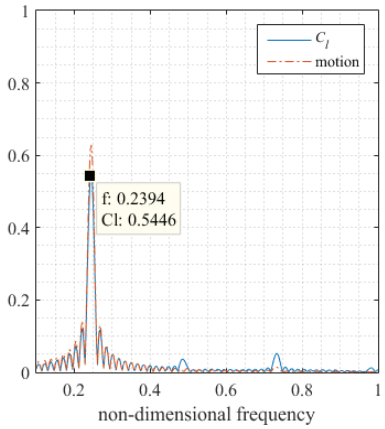

Fig.6. FFT analysis results (*KC*=4, α=45°, *G/D*=0.5)

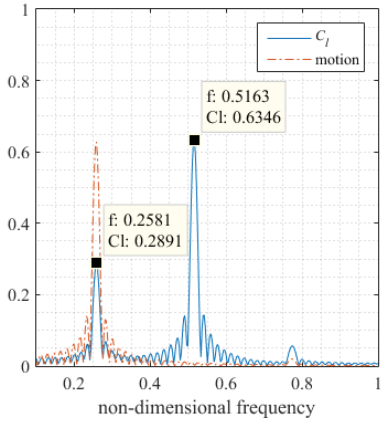

Fig.7. FFT analysis results (*KC*=4, α=75°, *G/D*=0.5)

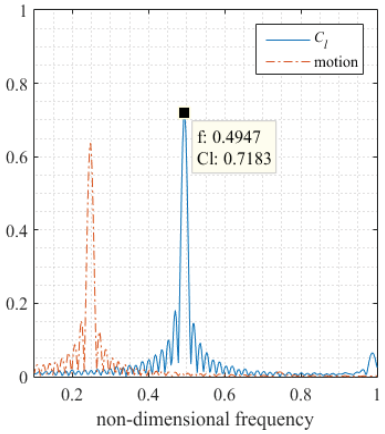

Fig.8. FFT analysis results (*KC*=4, α=90°, *G/D*=0.5)

As the 2nd frequency is approximately twice as high as the 1st frequency under each condition, each Fourier spectrum's frequency is divided by their own 1st frequency. For example, under 15°, the frequency is divided by 0.2391, under 75° the frequency is divided by 0.2581 to get the nth order oscillation frequency (the 1st frequency rounded to 1, the 2nd frequency rounded to 2, etc.). Combining the results in one 3D Figure, Fourier Spectrum's frequency order is shown in Fig.9.

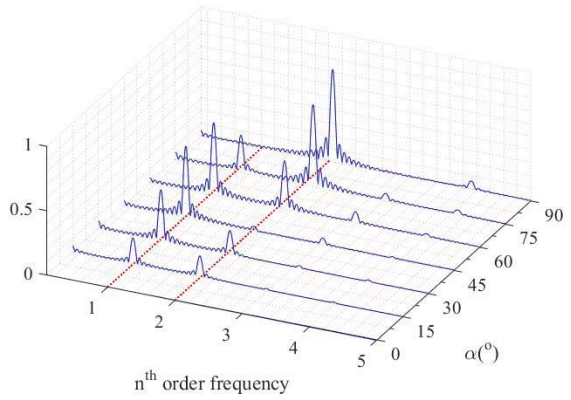

Fig.9 Combined FFT analysis results (*KC*=4, *G/D*=0.5)

In Fig.9, the red lines indicate where the 1st and 2nd order frequencies are. It further verifies the phenomena that both obvious 1st and 2nd frequency are observed except 45° where the 2nd frequency is very weak and 90° where the 1st frequency is very weak. Also, with the increase of α, the lift force coefficient's peak under the 1st frequency grows stronger at first until 45° and then declines when α grows bigger than 45°. Finally, it almost vanishes at 90°. In comparison, the peak under the 2nd frequency is restricted to a rather small scale when α is smaller than 45°, but gradually rises when α grows bigger than 45°. Finally, it almost dominates the entire spectrum when α= 90°.

In order to get more detailed information and explain such phenomena, flow field visualization is conducted to help shed some light on the discovery later in this paper.

B. *Drag Force Coefficient*

In fluid mechanics, the drag equation is expressed as,

$$F_d = \frac{1}{2}\rho u^2 C_d A \qquad (3)$$

Replacing the reference area A with the cylinder's diameter D, the right part of the drag equation converts to the drag force component in (1), where the drag force coefficient C_d is an important non-dimensional hydrodynamic coefficient that indicates whether the object under water will have more or less hydrodynamic drag. Through numerical simulation, the average drag force coefficient of Cylinder1 under each α and *G/D* is calculated and displayed in Fig.10 when *KC*=4. The dashed line signifies the single cylinder's C_d under the same *KC* and *Re*. Under the same *G/D*, the drag force coefficient C_d shows an overall trend of increase with α. Thus, cylinder pair under smaller α will have smaller drag force while cylinder pair under larger α will have larger drag force. Also, the gap ratio of 3.0 has the slowest trend of increase with α among all the gap ratios and is closest to the dashed line representing the single cylinder. Meanwhile, under *G/D*=0.5, the drag coefficient has the fastest trend of increase with α and deviates furthest from the line of single cylinder. Fan (2017) pointed out that this is because smaller gap ratios tend to enhance the interaction between two cylinders. Thus the energy outflow is stronger, which results in the enhancement of the drag force coefficient [6]. When the gap ratio grows bigger, the interaction between cylinders weakens and the hydrodynamic of each cylinder resembles that of single cylinder. Similar phenomena mentioned above could also be noticed under *KC* of 6 and 8, as shown in Fig,11 and Fig.12.

Furthermore, when α is bigger than 45°, C_d increases more rapidly with α than under 45°, especially when *G/D* is 0.5. Also, Fig.9 on the left shows that the 2nd frequency's rapid growth to domination occurs simultaneously when α>45°. Later in this paper, along with flow field visualization, an energy outflow calculation will be done to help analyze these phenomena.

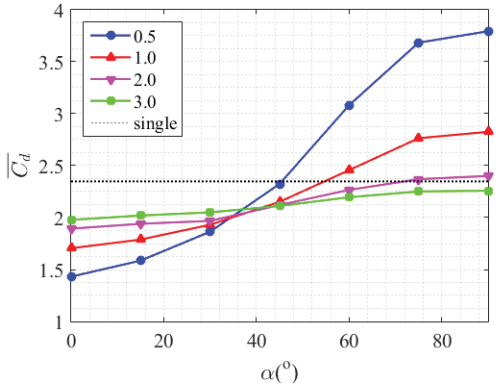

Fig.10 Average drag force coefficient (*KC*=4, *Re*=120)

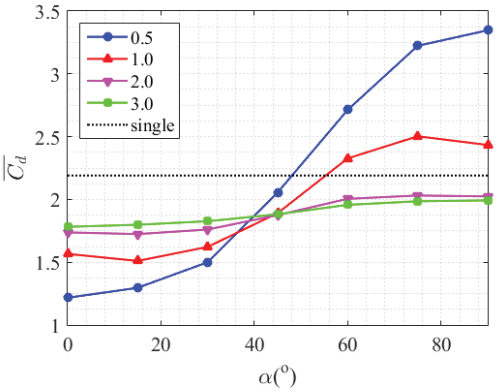

Fig.11 Average drag force coefficient (*KC*=6, *Re*=120)

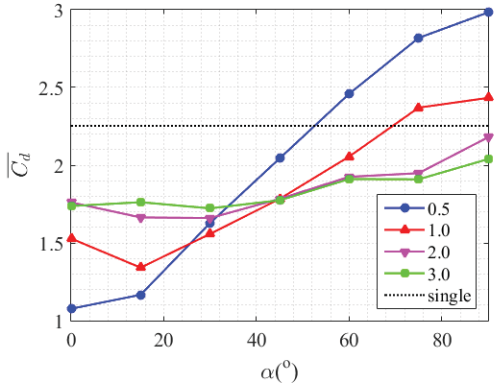

Fig.12 Average drag force coefficient (*KC*=6, *Re*=120)

IV. Flow Field Analysis

A. Lift Force Coefficient

The flow field of dual cylinders when α=0° arrangement is shown in Fig. 13, with *G/D*=0.5 and *KC*=4. Cylinder1 induces the vortex pair A, and Cylinder2 induces the vortex pair B. Due to the 'magnet' effect' [7], A and B connect, making the wake quite symmetrical, as shown in Fig.13. This verifies the discovery above that when α=0° (tandem arrangement), the lift force can barely be observed.

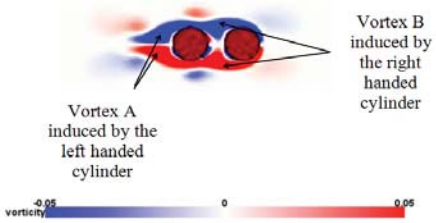

Fig. 13 flow field under tandem arrangement

As α increases, the flow pattern becomes different. Fig.14 shows the real-time lift force coefficient of Cylinder1 with time when α=15°. To better analyze the flow field and flow pattern, four non-dimensional characteristic time points are extracted where C_l reaches extreme value under the same α. Fig.15 shows the flow field at these time points when the vortex pattern has fully developed and becomes stable.

In Fig.14, C_l reaches its lowest point at 50.69. At the same time in the flow field, the cylinder pair is moving left. The vortex A induced by Cylinder1 and vortex B induced by Cylinder2 adhere to the cylinder pair's body in Fig.15 (a). Above the cylinders, the red part of A and B which have positive vorticity induced by both cylinders connect and form a bigger and stronger vortex, while beneath Cylinder1, the blue and negative part of the vortex is blocked and weakened in the gap, creating great asymmetry for Cylinder1 and enhancing the lift force to a bigger absolute value. When the cylinders move to the furthest left end and stop at 51.73, the vortex A and B shed out and move to the right region where vorticity is decaying, as shown in Fig. 15 (b). The new vortex adhering to the cylinders' body is not fully developed and the asymmetry becomes weaker so the absolute value of lift force coefficient decreases. Shortly, the cylinders start to move rightwards. As α (15°) is relatively small, the positive part of already-shed vortex B circulates around cylinder1 when the pair starts to move right. At the same time, Fig.14. shows a decrease in C_l from 51.73 to 52.33. This circulation changes the original flow field around cylinder1 and then affects the lift force. After the circulation ends, the new vortex C and D which adhere to the body while moving rightward grow stronger and begin to dominate the flow field. As the process is quite long and almost a half of the oscillation period, the lift force reaches its peak at 53.54, where the cylinders move to the furthest right. Although the vortex C induced in this half period will still circulate around after being shed, the circulation takes place around Cylinder2 and in this half period, the circulation has no significant influence on Cylinder1. The lift force reaches its lowest point again when the cylinders change its direction and move left. When this half period ends, next half period begins. The same flow pattern also takes place under α=30°. This flow pattern is identified as vortex circulation pattern.

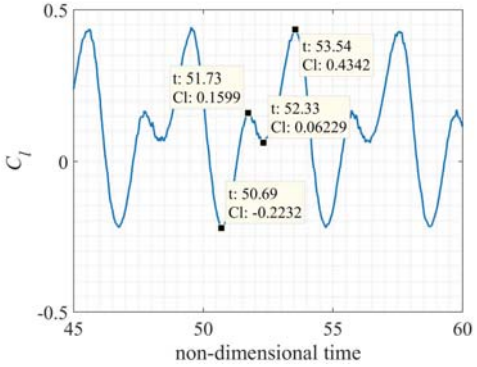

Fig. 14 Lift force coefficient with time (α=15°, *G/D*= 0.5 *KC*=4)

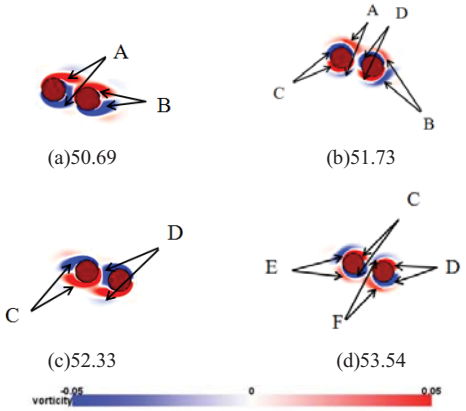

(a)50.69 (b)51.73

(c)52.33 (d)53.54

Fig. 15. Flow field analysis (α=15°, *G/D*= 0.5, *KC*=4)

When α>45°, the oscillation frequency of C_l is still twice as high as that of motion. However, the flow pattern is completely different. Fig.16 shows the real-time C_l of Cylinder1 during the oscillation. Although bigger α can barely make vortex circulate around Cylinder1's body after being shed, it enables the jet flow in the gap to be expelled far away, which can barely take place under small α as the cylinder has 'blockage effect' on jet flow when α is small, thus the vortex cannot be expelled far away. When the cylinders are moving left, as shown in Fig.17, vortex pair A and B adhere to the cylinder body at 50.34. Then cylinder pair moves to further left and stops at 51.56, vortex A and B are shed and the blue and negative part of vortex A which signifies negative vorticity is expelled in the gap along with the red and positive part of vortex B. At the same time point when vortices are shed, the lift force starts to change direction at 51.56. Then, the cylinder pair moves rightward at 52.53, when newly-induced vortex C and D adhere to the cylinder body. At 53.60, when cylinders move to the furthest right and stop, C and D are shed and the lift force starts to changes direction again. The newer vortex pairs E and F are induced and will adhere to the cylinder body in the next period while cylinder pair is moving leftward. Just like A and B, the vortex pairs E and F will be shed when the cylinder pair reaches furthest left. This half ends and the next period begins. The vortex is shed twice in one period, one at furthest left and the other at furthest right. Every time the vortices are shed, the

lift force changes direction. A vortex street can be seen on both sides of the gap. However, as the cylinder pair's center line is not precisely vertical to oscillation direction, the vortex street observed in Fig.17. is not precisely horizontal. In this paper, the flow pattern is defined as the jet flow pattern.

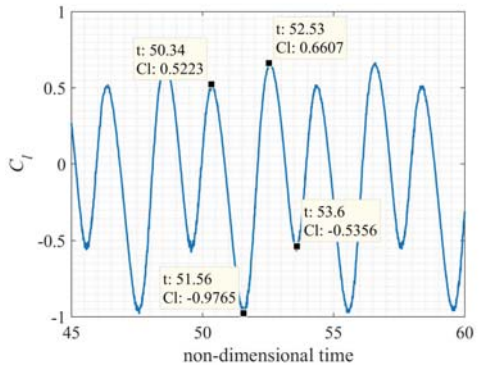

Fig. 16. Lift force coefficient with time (α=75°, *G/D* = 0.5, *KC*=4)

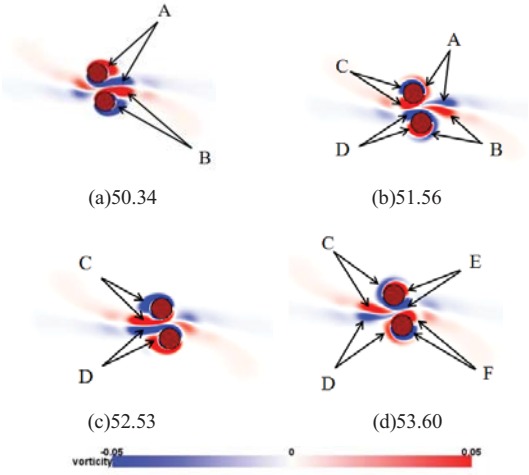

(a)50.34 (b)51.56

(c)52.53 (d)53.60

Fig. 17. Flow field analysis (α=75°, *G/D*= 0.5, *KC*=4)

When α reaches 90°, the 'blockage effect' by the other cylinder is alleviated. Fig. 18 shows the lift force with time. At 90° the same jet flow pattern takes place. At 50.45, the cylinder pair moves leftwards, convecting vortex A and B which adhere to the cylinder body to the left. At 51.57, the cylinder pair moves to the furthest left and stops. The vortex pairs A and B are shed and lift force starts to change direction. Then the cylinder pair moves rightward, convecting new adhering vortices C and D to the right, which will also be shed at 53.58 and expelled into the flow field far away, forming a vortex street in the gap between the cylinders. Again, the direction of the lift force changes following the shedding of C and D. The shedding of vortex takes place twice per period and the lift force coefficient's oscillation frequency is twice as high as that of motion when *KC*=4.

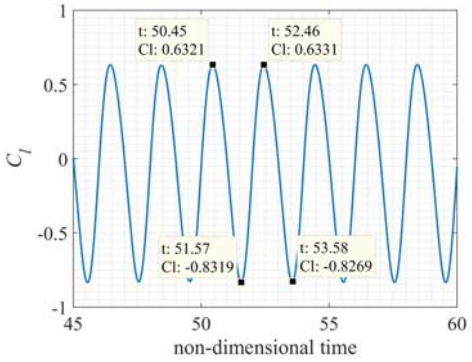

Fig. 18. Lift force coefficient with time (α=15° ,*G/D*= 0.5, *KC*=4)

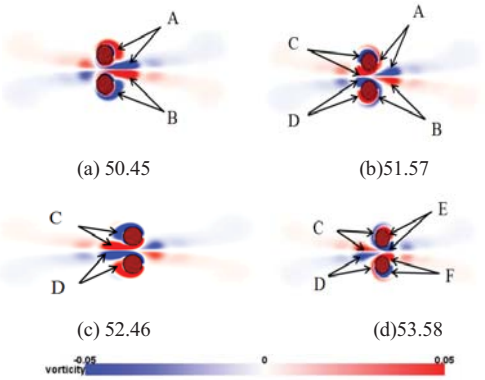

(a) 50.45 (b)51.57

(c) 52.46 (d)53.58

Fig. 19. Flow field analysis (α=90°, *G/D*=0.5, *KC*=4)

However, when α=45°, which is a critical condition, the vortex that has already been shed out can neither circulate around the upper cylinder nor be expelled far away in the gap, as shown in Fig.21. As a result, when the cylinder pair is moving leftwards at 50.52, vortex pairs A and B adhere to the cylinders body and the lift force is transitioning toward pointing down. When the cylinder pair reaches the furthest left at 51.43, vortex pair A and B are shed and the lift force reaches its biggest absolute value. Under 45°, the red and positive part of vortex B is hard to connect and perform circulation around Cylinder1 unlike 15° under which the circulation is observed. Instead, the already-shed vortex B is quickly neutralized by the wake. Thus unlike 15°, the 2nd frequency from C_l can barely be observed in the spectrum. When the cylinder pair is moving rightward at 52.51, the new vortex pair C and D adhere to the cylinder body and the lift force is gradually changing its direction and points upwards. Finally, it reaches its extreme value at 53.62 when the cylinder pair moves to furthest right. The vortex pair D will be quickly neutralized as well once shed out. Then newer vortex E and F appear and cylinder pair moves leftwards again. No obvious circulation nor vortex shedding takes place under 45° and C_l has the same angular frequency as that of motion, as shown in Fig.20.

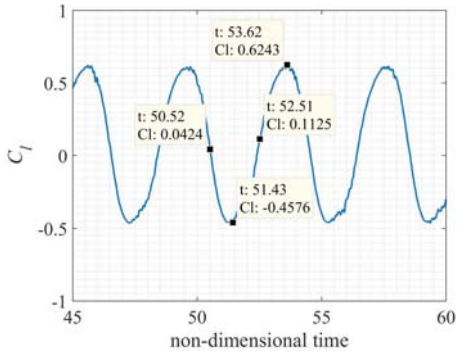

Fig. 20. Lift force coefficient with time (α=45°, *G/D*= 0.5, *KC*=4)

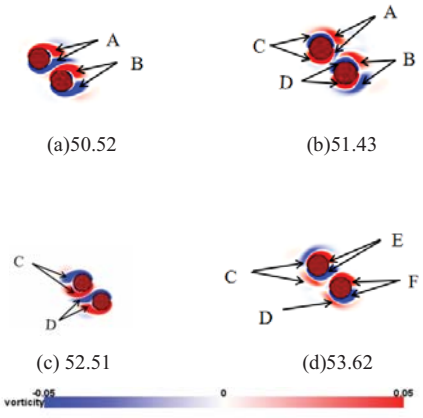

(a)50.52 (b)51.43

(c) 52.51 (d)53.62

Fig. 21. Flow field analysis (α=45°, *G/D* = 0.5, *KC*=4)

Such regular flow regimes when *KC*=4 will be influenced by bigger oscillation amplitude at higher *KC* number. Fig.22 (b) and (c) show the different flow patterns under *KC*=6 and 8 when the cylinder pair is moving left. Flow field at higher *KC* number tends to have more chaotic vortex pattern, especially at *KC* of 8 where the shaking of vortex wake can be easily observed. Future researches should be conducted for studying flow regimes under bigger *KC* and more complex vortex shedding patterns.

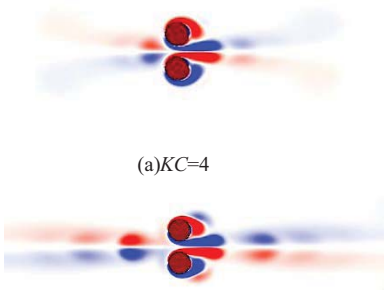

(a)*KC*=4

(b) *KC*=6

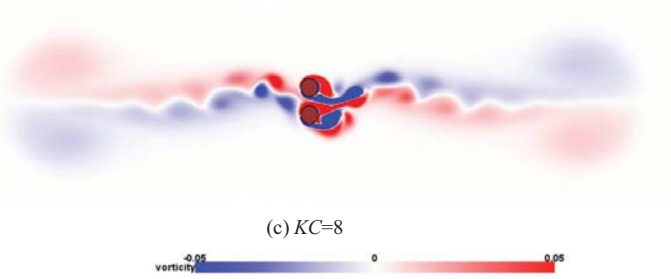

(c) *KC*=8

Fig. 22. Flow field (α=90°, *G/D*= 0.5)

B. *Drag Force Coefficient*

In (1), the drag component of in-line force with C_d signifies the non-conservative drag force that is related to energy dissipation while the other part with C_m signifies the inertial and conservative force [6]. In order to calculate the energy dissipation and further verify the enhancement of C_d with the increase of α, an energy outflow calculation is performed through the integration of kinetic energy about the control volume which includes the oscillating cylinders at every time point.

Fan (2017) calculated the Non-dimensional Energy Outflow Rate (*NEOR*) and verified the enhancement of drag force coefficient C_d in side-by-side arrangement under small *G/D* [6]. The *NEOR* is defined in (4) below,

$$NEOR = \oint \frac{1}{2}\left|\vec{u}\right|^2 \vec{u}\cdot\vec{n}ds \qquad (4)$$

$\vec{u}$ is the fluid particle's non-dimensional velocity vector on the boundary of control volume. $\vec{n}$ is the outward normal vector of control volume boundary. *ds* is the non-dimensional length of line between the neighbor nodes along the boundary of the control volume. Calculating *NEOR* can better monitor the amount of energy across the control volume carried by the vortex. In this paper, the time series of Non-dimensional Energy Outflow Rate (*NEOR*) under each α is calculated. The results of *NEOR* under *KC*=4 and *G/D*=0.5 is shown in Fig.23.

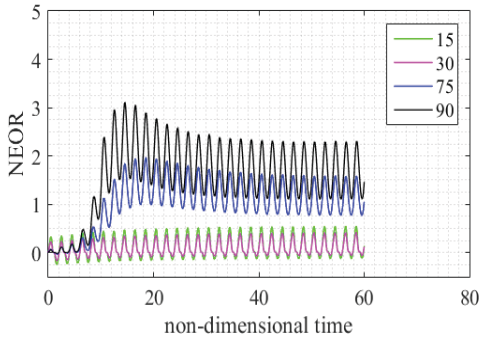

Fig.23. Non-dimensional Energy outflow rate (*KC*=4, *G/D*=0.5)

The time series of *NEOR* begins to jump from 0 and reaches a high value around which it starts to oscillate when α=90° and 75°. This indicates a jet flow carrying a larger amount of kinetic energy that reaches the boundary of the control volume during the oscillation when α=75° and 90°. This

jet flow could be easily observed in jet flow pattern under large α, as shown in Fig.24 (b), where the vortex pair A and B are expelled from the gap into the flow field far away carrying a large amount of energy. Also, the *NEOR* of 90° is notably stronger than that of 75°. However, no obvious enhancement of *NEOR* is observed when α is small as the *NEOR* of 30° almost overlaps with the *NEOR* of 15° in Fig.23. Under such conditions, flow field analysis in Fig.24 (a) shows that the vortex pair cannot be expelled far away due to the 'blockage effect' and no jet flow is observed.

To better illustrate the average energy outflow from each cylinder, the calculation of the mean *NEOR* for each cylinder, defined as mean *NEOR* of one period / Number of cylinders, is performed. The results are shown in Fig.25. The trend of mean *NEOR* agrees quite well with C_d under the same *KC* number, although when *KC*=4, it shows a slight decrease in the beginning. This may be related to the cylinders' alignment differences. Once α grows bigger than 45°, both C_d and Mean *NEOR* increase rapidly. As the drag force is related to the energy transfer and dissipation, the enhancement of the drag coefficient C_d could be the result of higher energy dissipation under large α.

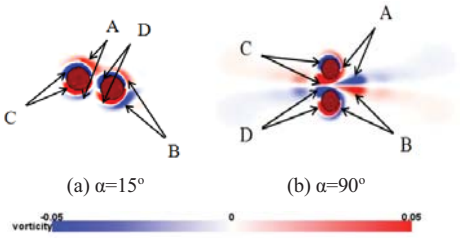

Fig.24. Flow field under two different patterns

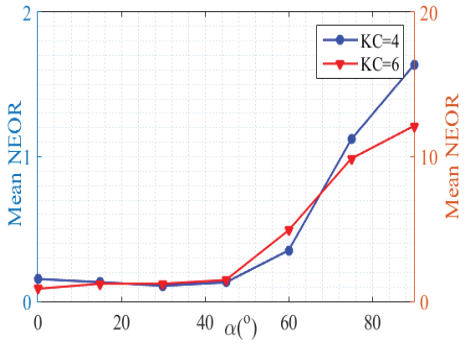

Fig.25. Mean NEOR

V. Conclusion

In this paper, numerical simulations on dual oscillating cylinders are conducted under different oscillation angles. Two hydrodynamic coefficients (C_d, C_l) are mainly chosen and analyzed. Double oscillation frequency has been found for the lift force coefficient C_l at all angles except 45° where C_l has the same frequency as that of motion. Meanwhile, smaller angle arrangement (mainly smaller than 45°) tends to weaken the drag force coefficient while the bigger angle (mainly bigger than 45°) tends to strengthen the drag force coefficient. Through flow field analysis, two major flow patterns for different angle arrangement are identified: the vortex circulation pattern when the angle is smaller than 45° and jet flow pattern when the angle is bigger than 45°. The vortex circulation pattern shows the circulation of vortex around the cylinder body after being shed, which arouses the 2nd frequency. The jet flow pattern shows that large angle arrangement enables the vortices to be shed twice per period in the gap, which arouses the 2nd frequency of C_l. Such shed-out vortices form jet flow in the gap that carries a large amount of energy away from the cylinder and enhance the energy dissipation. This is quantified by the calculation of Non-dimensional Energy Outflow Rate (*NEOR*). As the drag force is directly related to the energy dissipation, the sudden enhancement of drag force coefficient C_d under large angles could be explained by such expelled jet that only takes place under large angles. However, 45° is a critical arrangement under which the vortex can neither circulate nor shed far from the gap, making the oscillation frequency of C_l almost equal to that of motion.

References

[1] Morison, J. R., Johnson, J. W., & Schaaf, S. A. "The force exerted by surface waves on piles", *Journal of Petroleum Technology*, vol. 2(05), pp. 149-154, 1950

[2] Bearman, P. W., Graham, J. M. R., Downie, M. J., & Obasaju, E. D., "Forces on cylinders in viscous oscillatory flow at low Keulegan-Carpenter numbers", *Journal of Fluid Mechanics*, vol.154, pp. 337-356, 1985

[3] Sarpkaya, T. "Force on a circular cylinder in viscous oscillatory flow at low Keulegan—Carpenter numbers", *Journal of Fluid Mechanics*, vol. 165, pp. 61-71, 1986

[4] Williamson, C. H. K. "Sinusoidal flow relative to circular cylinders. Journal of Fluid Mechanics", *Journal of Fluid Mechanics*, vol. 155, pp. 141-174, 1985.

[5] An, H., Cheng, L., & Zhao, M., "Steady streaming around a circular cylinder in an oscillatory flow", *Ocean Engineering,* vol. 36(14), pp. 1089-1097, 2009.

[6] Fan, D., Zhang, X. and Triantafyllou, M.S., "Drag coefficient enhancement of dual cylinders in oscillatory flow", *ISOPE 2017-San Francisco,* 2017.

[7] Zhang X., Fan D. &Wan D., "Numerical study of oscillatory dual cylinders in tandem arrangement", *ISOPE 2017-San Francisco*, 2017

[8] Weymouth, G. D., & Yue, D. K., "Boundary data immersion method for Cartesian-grid simulations of fluid-body interaction problems", *Journal of Computational Physics*, vol. 230(16), pp. 6233-6247, 2011.

[9] Tong F., Cheng L. and Zhao M., "Oscillatory flow regimes around four cylinders in a square arrangement under small *KC* and *Re* conditions", *Journal of Fluid Mechanics*, vol. 769, pp. 298–336, 2015.